Mendeleev Communications

Mendeleev Commun., 2026, **36**, 79–81

Novel naphthalene benzimidazole-based materials for potassium metal batteries: revealing the importance of molecular weight for material performance

Yuriy I. Baluda,[a] Alexander V. Mumyatov,[a] Tatyana A. Savinykh,[a] Evgeniya P. Antoshkina,[b,c] Sergey G. Vasil'ev,[a] Alexander F. Shestakov,[a,d] Pavel A. Troshin[e,a] and Olga A. Kraevaya*[a]

[a] *Federal Research Center of Problems of Chemical Physics and Medicinal Chemistry, Russian Academy of Sciences, 142432 Chernogolovka, Moscow Region, Russian Federation. E-mail: okraevaya@inbox.ru*
[b] *A. N. Nesmeyanov Institute of Organoelement Compounds, Russian Academy of Sciences, 119334 Moscow, Russian Federation*
[c] *Moscow Institute of Physics and Technology (National Research University), 141701 Dolgoprudny, Moscow Region, Russian Federation*
[d] *Department of Fundamental Physical and Chemical Engineering, M. V. Lomonosov Moscow State University, 119991 Moscow, Russian Federation*
[e] *Zhengzhou Research Institute, Harbin Institute of Technology, 450003 Zhengzhou, China*

DOI: 10.71267/mencom.7719

A family of novel naphthalene benzimidazole (NBI)-based materials with different molecular weights was prepared by condensing 1,4,5,8-naphthalenetetracarboxylic dianhydride with 2,3-diaminophenazine, 2,3,7,8-tetraaminophenazine or their mixture. Of these materials, only intermediate molecular weight NBI provides high specific discharge capacity and exhibits good cycling stability and rate capability in potassium cells, while polymeric NBI also demonstrated decent performance in lithium cells. The results suggest a new approach for further rational design of NBI materials for metal-ion batteries with improved performance.

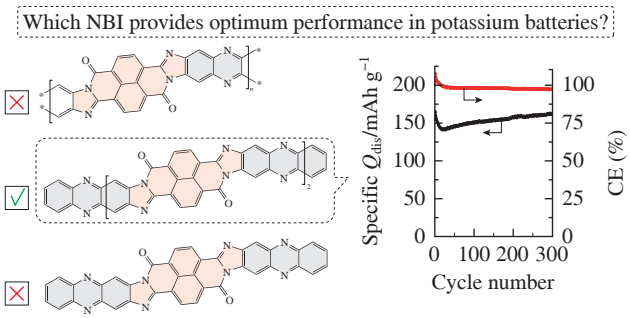

Keywords: organic electrode materials, lithium metal battery, potassium metal battery, 1,4,5,8-naphthalenetetracarboxylic dianhydride, aminophenazines, polyimides, naphthalene benzimidazoles.

Organic electrode materials (OEMs) are considered as a promising alternative to traditional inorganic cathode materials used in metal-ion batteries. Their low cost, high specific capacity, ease of recycling, environmental friendliness, charge–discharge cycling stability and good mechanical properties may lead to the development of a game-changing battery technology. An undeniable advantage of OEMs is their ability to incorporate cations of not only lithium, but also other metals more common in the earth's crust and seawater, including sodium, potassium, zinc, aluminum, *etc*.[1] Sodium and potassium exhibit electrochemical and chemical properties close to lithium, which allows the fabrication of batteries with a specific capacity and average voltage not inferior to lithium analogues. Thus, sodium, potassium and zinc-ion systems are very promising for commercialization, especially for the development of safe on-grid energy storage devices.

Redox-active OEMs in metal-ion batteries typically contain moieties such as sulfide,[2] carbonyl[3] and imine groups, nitroxyl radical centers[4] and aromatic amines.[5] Small organic molecules are rarely used due to their solubility in the electrolyte, which further reduces cycling stability. One of the most effective strategies for inhibiting dissolution is the synthesis of redox-active polymers. Polyimides are among the most widely used redox-active carbonyl polymers due to their satisfactory capacity, excellent cycling performance and good rate capability. In addition, polyimides are used as coatings, separators, binders and solid-state electrolytes in lithium-ion batteries, as well as bipolar plate materials in hydrogen fuel cells.[6] Polyimides derived from 1,4,5,8-naphthalenetetracarboxylic dianhydride (NDA) have excellent mechanical strength, high thermal stability and chemical inertness[7] and are classified into aliphatic and aromatic. Aliphatic NDA-based polyimides are widely used as active OEMs.[8] In contrast, the more rigid and insoluble aromatic polyimides are used primarily as membranes or electrodes.[9] Aromatic polyimides with a rigid ladder-type structure can be obtained by condensation of NDA and tetraamines, leading to the formation of benzimidazole fragments.[10]

Monomeric naphthalene benzimidazoles (NBIs) have been previously used as ligands for red phosphorescent cyclometalated iridium(III) complexes,[11] chemosensors for fluoride ion (F^-) detection,[12] acceptor molecules for OPV devices[13] and n-type semiconductors for OFETs[14] and represent a class of materials promising for electrochemical applications. Here we report the design and optimization of NBIs derived from NDA and aminophenazines and their investigation as cathode materials for lithium- and potassium-ion batteries.

Condensation of NDA with 2,3,7,8-tetraaminophenazine **1**, 2,3-diaminophenazine **2** or a 1 : 2 mixture of them in *N*-methylpyrrolidone (NMP) afforded the materials **NBI1**, **NBI3** and **NBI2** (Scheme 1), rerspectively, with very limited solubility in

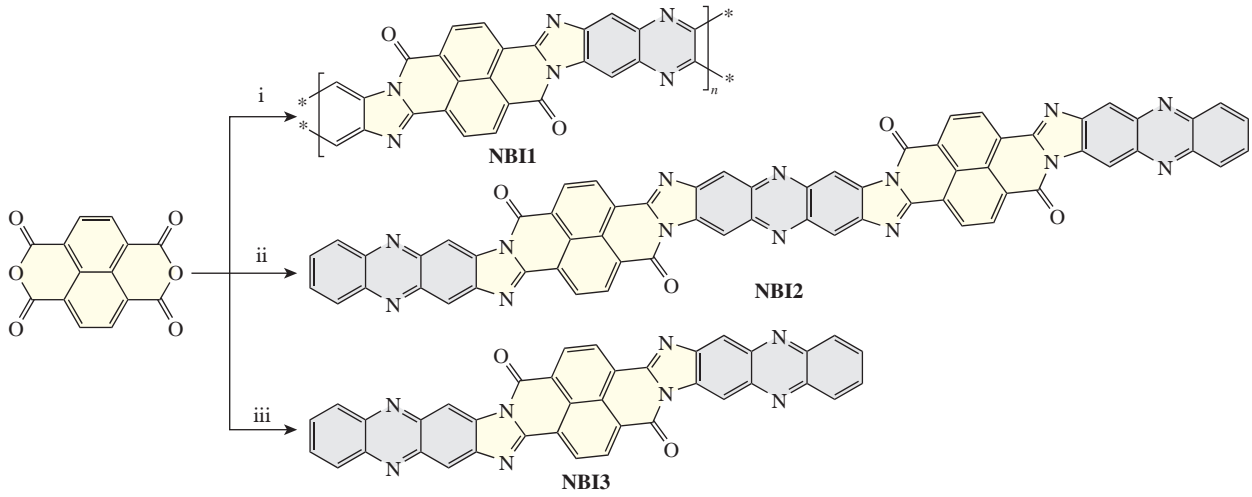

Scheme 1 *Reagents and conditions*: i, **1**, NMP, reflux, 6 h; ii, **1** + **2**, NMP, reflux, 6 h; iii, **2**, NMP, reflux, 6 h.

toluene, diethyl carbonate and NMP. Due to low solubility issues, all materials were characterized using solid-state methods (Figures S1–S10, see Online Supplementary Materials).†

First, cells with lithium anodes and 1 M LiTFSI electrolyte were assembled‡ and characterized by cyclic voltammetry (CV) and galvanostatic cycling (Figures S11–S13). The CV curve of Li//**NBI1** [Figure 1(*a*)] demonstrates a broad oxidation wave between 2.5 and 2.7 V and a reduction wave at 2.2–2.4 V *vs.* Li^+/Li. These potential values are typical for materials containing carbonyl groups. Another reduction peak with a potential of ~1.5 V is attributed to the redox processes involving the C=N bonds of the phenazine moieties. Since **NBI1**–**NBI3** contain the same types of redox centers, their CV curves in lithium cells were quite similar. Compared with the CV curve of the **NBI3**-based cell [Figure S13(*a*)], the **NBI2**-based system [Figure S12(*a*)] showed better cycle-to-cycle reproducibility, indicating that fewer irreversible parasitic processes occur in the **NBI2** cathode during reduction and oxidation.

Galvanostatic charge–discharge cycling of Li//**NBI1** cells at a current density of 100 mA g^{-1} [Figure 1(*b*)] revealed a maximum capacity of ~170 mAh g^{-1}, which decreased to 125 mAh g^{-1} after 200 charge–discharge cycles. The observed cell activation behavior, manifested by an increase in capacity and an increase in CV currents during the first tens of cycles, is most likely due to an increase in the accessibility of the redox centers. To overcome the kinetic difficulties and fully elucidate the potential of the material, a charge–discharge test in the CCCV (constant current–constant voltage) mode was performed with Li//**NBI1** cells [Figure S11(*c*),(*d*)]. The potentiostatic stage ensures a better charge distribution in the electrode volume and a more complete utilization of the active material. Indeed, a pronounced growth of the discharge capacity (Q_{dis}) up to 242 mAh g^{-1} was observed during the first 10 cycles. After 75 cycles, the specific Q_{dis} value exceeded 190 mAh g^{-1}, accompanied by a Coulombic efficiency (CE) close to 100%. The charge–discharge curves showed a significant contribution (~50%) of the potentiostatic stage to the Q_{dis} value at the 10th cycle and its further decrease to ~10% at the 75th cycle. Since the possibility of upscaling is critically important for energy storage systems, pouch-type cells with Li anodes and **NBI1** cathodes were fabricated. Specific Q_{dis} of 166 mAh g^{-1} was achieved in this system after 100 cycles [Figure S11(*b*)], which is slightly better than the result obtained with coin cells under the same cycling conditions.

Lithium cells with **NBI2**-based cathodes demonstrated rather similar behavior (maximum Q_{dis} of ~200 mAh g^{-1} and Q_{dis} of ~100 mAh g^{-1} after 200 cycles), while for **NBI3** the results of galvanostatic cycling were less promising, as the capacity of the material dropped sharply to ~80 mAh g^{-1} after 200 cycles. Such behavior is very typical for materials that form soluble metalation products during cycling. The slow capacity decrease for **NBI1**- and **NBI2**-based cathodes may be a result of partial degradation

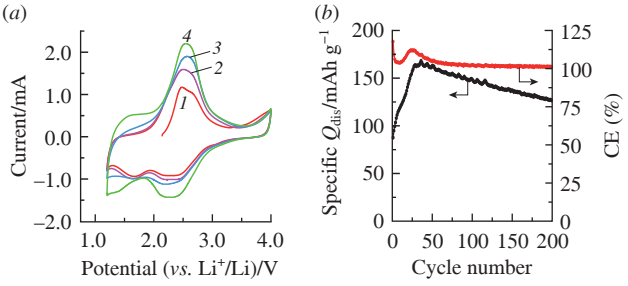

Figure 1 Characterization of the Li//**NBI1** cell: (*a*) CV curves for (*1*) 1st, (*2*) 2nd, (*3*) 5th and (*4*) 10th scans; (*b*) cycling performance at a current density of 100 mA g^{-1}.

† In the FTIR spectrum of **NBI3**, the absorption bands attributed to the vibrations of the anhydride C=O bonds in the starting material NDA (1762 cm^{-1}) almost completely disappear as a result of the successful condensation of NDA with 2,3-diaminophenazine. For **NBI2**, the residual signals of the anhydride C=O bond vibrations are more pronounced, indicating the presence of terminal anhydride groups (see Figure S1). Since a mixture of tetra- and diaminophenazines in a 1 : 2 molar ratio was used for the synthesis of **NBI2**, it represents a statistical mixture of oligomers, some of which may be terminated with anhydride or carboxyl groups. In the FTIR spectrum of the polymer **NBI1**, these signals are even more pronounced. The FTIR spectra of **NBI1**–**NBI3** also reveal a strong characteristic 'amide-I' band at 1695–1700 cm^{-1}, which proves the formation of the NBI moiety. The ^{13}C ssNMR spectra of **NBI1**–**NBI3** are quite similar, with two major signals at 130 and 141–142 ppm, which are expected for NBIs. Some minor signals are also observed at 170–180 ppm, indicating the presence of carbonyl groups (Figures S3, S5 and S7). The MALDI mass spectra of the polymer **NBI1** (Figure S8) revealed a signal of the monomeric unit (M) $[M + H]^+$ with $m/z = 437.36$ (calculated for $[C_{26}H_8N_6O_2 + H]^+$: 437.08). For **NBI2**, small oligomers with different NDA/phenazine ratios were identified in the MALDI mass spectrum (Figure S9). Oligomers with molecular weights more than 1 kDa were not detected, most likely due to their fragmentation. As expected for the small-molecule material **NBI3**, the mass spectra revealed a major signal of the molecular ion $[M]^-$ with $m/z = 616.24$ (calculated for $[C_{38}H_{16}N_8O_2]^-$: 616.14) along with signals from some minor products with free amino and carbonyl groups (Figure S10).

‡ Since the as-synthesized materials usually have suboptimal particle sizes, all materials were ball milled in an aqueous medium and lyophilized. The resulting powders were thoroughly mixed with conductive carbon and PVDF binder and dispersed in NMP. The obtained slurries were tape-cast onto carbon-coated aluminum foil, dried and calendered. Circular electrodes for CR2032-type cells were cut out and subsequently used to fabricate batteries.

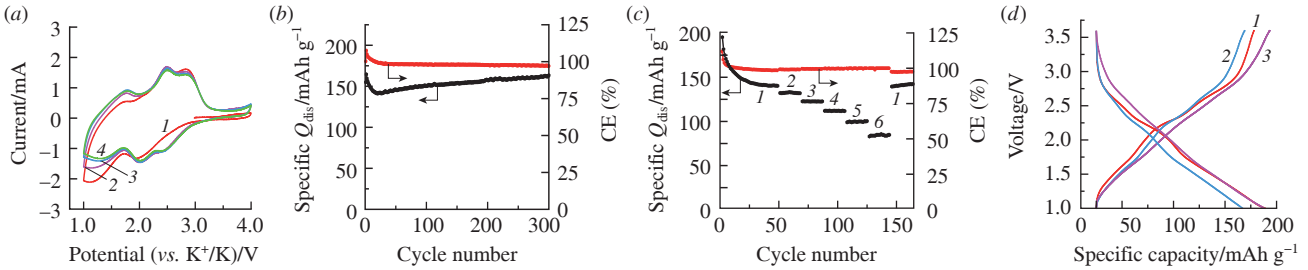

Figure 2 Characterization of K//**NBI2** cells: (*a*) CV curves for (*1*) 1st, (*2*) 2nd, (*3*) 5th and (*4*) 10th scans; (*b*) cycling performance at a current density of 100 mA g^{-1}; (*c*) rate capability at a current density (mA g^{-1}): (*1*) 100, (*2*) 200, (*3*) 400, (*4*) 800, (*5*) 1600 and (*6*) 3200; (*d*) charge–discharge curves at a current density of 100 mA g^{-1} after (*1*) 2, (*2*) 30 and (*3*) 300 cycles.

of the active material during cycling followed by solubilization of low-molecular-weight degradation products, as previously noted for other polyimides.[15] Thus, for the fabrication of lithium-ion batteries, it is preferable to use higher molecular-weight redox-active materials with low solubility in electrolytes.

To investigate the influence of the molecular structures of **NBI1**–**NBI3** on their performance in potassium cells, we fabricated cells with potassium-based anodes and KPF_6 electrolyte. Unfortunately, **NBI1**- and **NBI3**-based cells demonstrated low Q_{dis} values and a high proportion of short-circuited cells, while the galvanostatic cycling results of K//**NBI2** cells were even more promising compared to Li-based systems (Figure 2). **NBI2**-based potassium cells showed a slight initial capacity decrease to 135 mAh g^{-1}, then the capacity slowly increased and reached 165 mAh g^{-1} without any signs of degradation after 300 cycles [Figure 2(*b*),(*d*)]. As expected, the CV curves confirmed that carbonyl and partly phenazine groups are involved in redox processes [Figure 2(*a*)]. The rate capability of potassium cells was also better than that of lithium systems: with a gradual increase in current density from 100 to 3200 mA g^{-1} [Figure 2(*c*)], the specific Q_{dis} value of potassium cells decreased from 135 to 80 mAh g^{-1}, while for **NBI2**-based lithium cells it dropped from 170–175 to 25 mAh g^{-1}. The composition of **NBI1**- and **NBI3**-based potassium cells was optimized using a dendrite-free anode based on a liquid K–Na alloy. Although the optimized cells demonstrated more stable behavior, the Q_{dis} values achieved in these systems did not exceed 75 mAh g^{-1} after 200 cycles (Figures S14 and S15).

Thus, compared with the polymer material **NBI1** and the small-molecule material **NBI3**, the oligomeric material **NBI2** obtained by three-component condensation demonstrated more promising performance as a cathode component in potassium-ion batteries. The polyimide **NBI2** outperforms most polyimides previously investigated in potassium cells in terms of specific capacity and cycling stability (Table S1, see Online Supplementary Materials). To the best of our knowledge, our work is the first to apply NBI derivatives as electrode materials in potassium-ion batteries.

To better understand the metalation processes of the obtained NBIs, quantum chemical calculations were performed. The calculation of the band gaps showed that **NBI1** should have better conductivity compared to **NBI2** and **NBI3** (Figures S16 and S17). The investigated materials have three types of redox-active sites, such as C=O, N–C=N and pyrazine rings (Figures S18 and S19). The highest binding energies during the coordination of Li^+ and K^+ are observed for the C=O groups, and lower (by 0.2 and 0.3 eV for Li^+ and K^+, respectively) are for the N–C=N groups. For the pyrazine moiety, the binding energies are comparable with those for the N–C=N groups (in the case of Li^+) or slightly lower (by 0.1 eV in the case of K^+). Thus, the carbonyl sites are more favorable for the coordination of ions during the metalation of NBIs, which is consistent with the CV results.

In summary, we designed, synthesized and characterized a series of redox-active materials **NBI1**–**NBI3** containing naphthalene benzimidazole moieties. The resulting NBIs were investigated as cathode materials for lithium and potassium batteries and demonstrated decent discharge capacities. However, in terms of cycling stability, rate capability and discharge capacity, the best results were achieved in potassium metal batteries with the material prepared by condensation of NDA and a mixture of tetra- and diaminophenazines. These results underline the importance of material design and structure optimization for the development of metal-ion batteries with polyimide electrodes.

This work was supported by the Ministry of Science and Higher Education of the Russian Federation [project no. FFSG-2025-0005 (125032604442-5)].

Online Supplementary Materials

Supplementary data associated with this article can be found in the online version at doi: 10.71267/mencom.7719.

References

1 P. M. H. Prasad, G. Malavika, A. Pillai, S. Sadan and Z. S. Pillai, *NPG Asia Mater.*, 2024, **16**, 37; https://doi.org/10.1038/s41427-024-00557-5.
2 W. Sun, J. Ying, Z. Huang, C. Jiang and C. Wan, *Prog. Chem. (Beijing, China)*, 2009, **21**, 1963; https://manu56.magtech.com.cn/progchem/EN/Y2009/V21/I09/1963#2.
3 Z. Song, Y. Qian, X. Liu, T. Zhang, Y. Zhu, H. Yu, M. Otani and H. Zhou, *Energy Environ. Sci.*, 2014, **7**, 4077; https://doi.org/10.1039/C4EE02575J.
4 Q. Yu, Z. Xue, M. Li, P. Qiu, C. Li, S. Wang, J. Yu, H. Nara, J. Na and Y. Yamauchi, *Adv. Energy Mater.*, 2021, **11**, 2002523; https://doi.org/10.1002/aenm.202002523.
5 Y. Tong, Y. Wei, A. Song, Y. Ma and J. Yang, *ChemSusChem*, 2024, **17**, e202301468; https://doi.org/10.1002/cssc.202301468.
6 N. S. Eroshenko, V. E. Andreeva, O. A. Medennikov and N. V. Smirnova, *Mendeleev Commun.*, 2024, **34**, 342; https://doi.org/10.1016/j.mencom.2024.04.010.
7 M. Zhang, L. Wang, H. Xu, Y. Song and X. He, *Nano-Micro Lett.*, 2023, **15**, 135; https://doi.org/10.1007/s40820-023-01104-7.
8 J. Wang, H. Liu, C. Du, B. Liu, H. Guan, Y. Liu, S. Guan, Z. Sun and H. Yao, *eScience*, 2024, **4**, 100224; https://doi.org/10.1016/j.esci.2023.100224.
9 J. Wang, H. Liu, C. Du, X. Zhang, Y. Liu, H. Yao, Z. Sun and S. Guan, *Chem. Eng. J.*, 2022, **444**, 136598; https://doi.org/10.1016/j.cej.2022.136598.
10 J. Mizuguchi, *J. Phys. Chem. B*, 2004, **108**, 8926; https://doi.org/10.1021/jp031351d.
11 P. Rajakannu, H. S. Kim, W. Lee, A. Kumar, M. H. Lee and S. Yoo, *Inorg. Chem.*, 2020, **59**, 12461; https://doi.org/10.1021/acs.inorgchem.0c01561.
12 D. Li, Z. Zhong, G. Zheng and Z. Tian, *Spectrochim. Acta, Part A*, 2017, **185**, 173; https://doi.org/10.1016/j.saa.2017.05.053.
13 M. Javed, A. Farhat, S. Jabeen, R. A. Khera, M. Khalid and J. Iqbal, *Comput. Theor. Chem.*, 2021, **1204**, 113373; https://doi.org/10.1016/j.comptc.2021.113373.
14 M. Mamada, C. Pérez-Bolívar, D. Kumaki, N. A. Esipenko, S. Tokito and P. Anzenbacher, Jr., *Chem. – Eur. J.*, 2014, **20**, 11835; https://doi.org/10.1002/chem.201403058.
15 A. F. Shestakov, O. V. Yarmolenko, A. A. Ignatova, A. V. Mumyatov, K. J. Stevenson and P. A. Troshin, *J. Mater. Chem. A*, 2017, **5**, 6532; https://doi.org/10.1039/C6TA10520C.

Received: 9th January 2025; Com. 25/7719